Lawrence Berkeley Laboratory
UNIVERSITY OF CALIFORNIA

Materials & Molecular Research Division

HIGH-TEMPERATURE OXIDATION AND CORROSION OF MATERIALS PROGRAM

David P. Whittle

March 1980

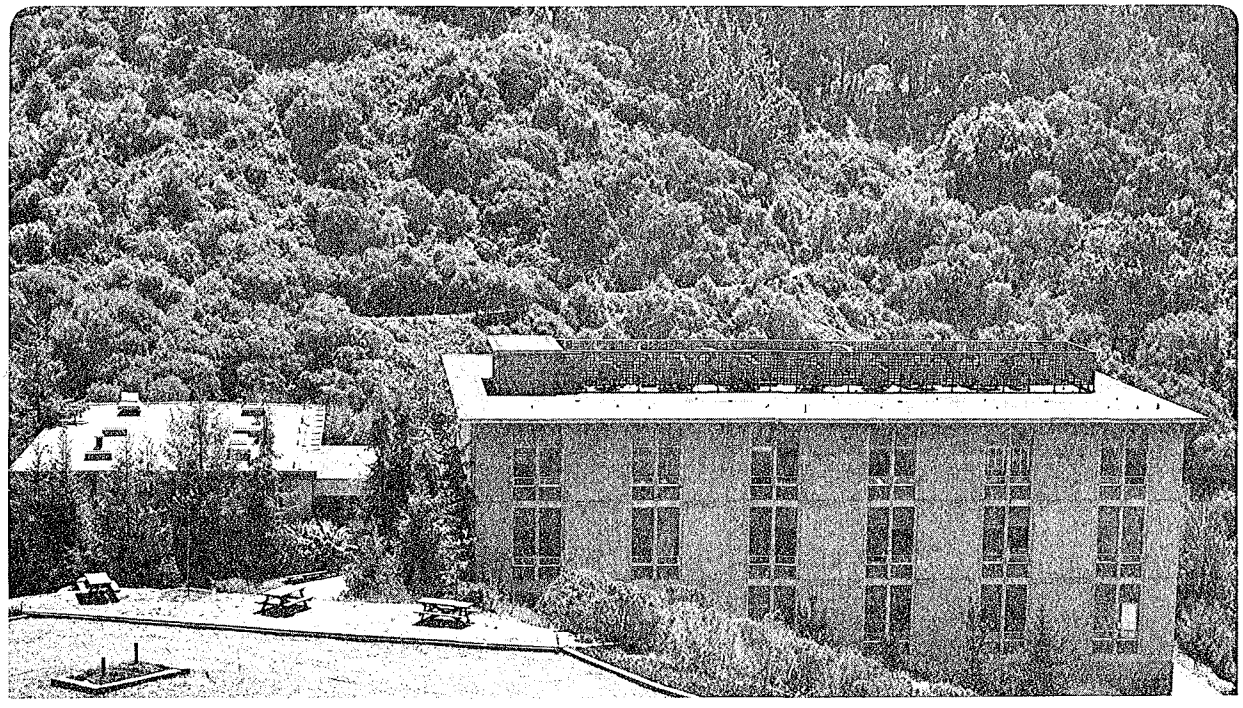

Prepared for the U.S. Department of Energy under Contract W-7405-ENG-48

LBL-11202

HIGH-TEMPERATURE OXIDATION AND CORROSION OF MATERIALS PROGRAM

David P. Whittle

Materials and Molecular Research Division
Lawrence Berkeley Laboratory
University of California
Berkeley, California 94720

Excerpt from LBL-10000

Lawrence Berkeley Laboratory
University of California
Berkeley, California 94720
Telephone 415/486-4000
FTS: 451-4000

June 23, 1980

Dear Colleague:

Please find attached a summary of my group's research over the last year in high temperature corrosion. This was originally prepared for our Divisions' annual report. However, much of the work has been published in more detail either in referred journals or as reports and copies are available in request.

Please feel free to contact me with any questions relating to the work.

Yours sincerely,

Professor D.P. Whittle

DPW/baj

Enclosure

f. High Temperature Oxidation and Corrosion of Materials*

David P. Whittle, Investigator

Introduction. The objective of this program is to gain an understanding of the corrosion chemistry and materials behavior in high temperature environments. Of particular interest are the mechanisms of attack in environments containing more than one reactive species, for example sulfur and oxygen. Sulfur is a critical impurity in almost all energy sources and leads to accelerated, and often unacceptable rates of metal degradation. In addition, the competitive formation of potentially more than one phase as a reaction product is an important fundamental problem, and can only be truly understood if the underlying thermodynamic and transport properties of the systems, and their interrelation, are identified. Sulfur can appear in a number of forms. In entirely gaseous environments it can appear as H_2S when the oxidizing potential of the atmosphere is low, such as might exist in energy conversion systems, or as SO_2/SO_3 at higher oxygen potentials, such as those produced by fuel combustion. It may also appear in sulfatic deposits, either as a solid, such as $CaSO_4$ in fluidized bed combustion systems, as inorganic and organic sulfur compounds in coal char, or as a liquid alkali-metal sulfate in coal-ash, or turbine-blade deposits. This last year has been spent primarily in establishing the typical behavioral patterns of common materials in these types of environments, and identifying the common mechanisms. In addition, development of definitive models of alloy reactions with single oxidants has continued. The individual projects are described below.

1. EQUILIBRIA IN GASEOUS SYSTEMS

D. P. Whittle, I. M. Allam, and H. Hindam

Correct interpretation of the behavior of metals and alloys in multicomponent gas mixtures at high temperature requires that the equilibrium conditions in the gas phase be known. In addition, it is also important to establish how the composition of the gas mixture, assuming it is at equilibrium, and in particular how the activities of the oxygen and sulfur reactants will change when one of the components is removed from the gas by reaction with the metal. This may not be critical in flowing, well-mixed systems, but where stagnant pockets of gas can exist, such as beneath inert deposits, in crevices, or within porous scales, it can have serious consequences.

In the S-O-H system, there are at least 14 possible gaseous species: H_2, O_2, S_2, S_4, S_8, H_2O, SO_2, SO_3, SO, O, H, S, OH, etc. However, in the temperature, pressure and overall gas composition ranges of interest in the present context, sulfur species higher than the dimer, atomic oxygen, hydrogen and sulfur, and free radicals such as OH can be neglected. The equilibrium composition of any gas mixture is calculated through the equilibrium constant approach. In essence two types of equations are involved: Mass balance equations which ensure that the total content of the three atomic species are conserved, and the intergaseous equilibria. A computer program has been written to solve the system of eight, nonlinear simultaneous equations for any given input composition. Solutions have been obtained at temperatures in the range 600-1200°C intervals, for a total system pressure of 1 atm. and for input compositions covering the whole range of oxygen and hydrogen contents and up to a sulfur level equivalent to 10% H_2S or SO_2. Table 1 shows a sample output. Figure 1 shows the P_{S_2} in the equilibrated gas as a function of P_{O_2} at 1000°C for four different sulfur levels and a number of different oxygen levels.

As a whole, the S-O-H system can be divided into three sectors depending on the relative amounts of oxygen, sulfur and hydrogen in the gas mixture, best expressed as N_O, N_S and N_H where N_i is the fraction of total atoms of species i. At low oxygen contents, $N_S + N_O \leq 1/3$, H_2S-H_2O-H_2 are the major molecular species: the sulfur and oxygen potentials are relatively independent with the sulfur potential decreasing slightly with decreasing oxygen potential at a fixed sulfur content. At intermediate oxygen and sulfur contents, $N_S + N_O \geq 1/3$, $N_S \leq 1/3$ and $N_O - N_S \leq 1/3$, H_2O-H_2S-SO_2 are the major molecular species, and within this region sulfur and oxygen potentials are strongly interrelated, being inversely proportional to one another. In the third sector, $N_O - N_S \leq 1/3$, O_2-SO_2-H_2O are the major species; sulfur potentials are very low, and again are independent of oxygen potential.

These interdependencies between the sulfur and oxygen potentials have a considerable influence on likely corrosion behavior. The regime in which sulfur and oxygen potentials are strongly interdependent represents a very small change in overall composition, corresponding to almost exact, stoichiometric combustion of a fuel for example, and most practical combustion environments would be more oxygen-rich. It is nevertheless important since regions of stagnant gas within porous deposits or crevices, for example, could approach these conditions by reacting with oxygen to form oxides. In this context, the buffering capacity of the gas, or its ability to resist a change in sulfur potential caused by removal of oxygen in reaction is critical. These buffering capacities can be calculated from the equilibrated compositions computed above, and are equally important in determining corrosion behavior as the often quoted sulfur and oxygen potentials.

An additional feature evident from the calculations is the relative position of the maximum in sulfur potential as a function of oxygen potential with respect to the stabilities of the sulfides and oxides of the common alloying elements, Ni, Co, Cr, Fe, Al, etc. With the Ni-S-O system the maximum

*This work was supported by the Division of Materials Sciences, Office of Basic Energy Sciences, U. S. Department of Energy.

Table 1. Equilibrated compositions in the S-O-H system; input composition: H_2S = 8.9%, H_2O = 90.1%, SO_2 = 1.0%, N_S = 0.033, N_H = 0.66, and N_O = 0.307.

TEMP(C)	H2S	H2O	SO2	H2	SO3	SO	O2	S2
600.	-1.0737	-.0442	-2.0527	-2.6350	-10.4114	-6.4515	-18.6849	-2.5416
650.	-1.0816	-.0442	-2.0492	-2.3996	-10.1494	-6.0467	-17.5553	-2.4441
700.	-1.0917	-.0445	-2.0365	-2.1916	-9.9007	-5.6783	-16.5333	-2.3544
750.	-1.1047	-.0450	-2.0135	-2.0081	-9.6597	-5.3393	-15.6010	-2.2707
800.	-1.1210	-.0457	-1.9805	-1.8465	-9.4236	-5.0252	-14.7444	-2.1924
850.	-1.1409	-.0467	-1.9387	-1.7042	-9.1914	-4.7328	-13.9529	-2.1198
900.	-1.1648	-.0481	-1.8902	-1.5788	-8.9634	-4.4602	-13.2182	-2.0537
950.	-1.1929	-.0497	-1.8369	-1.4681	-8.7407	-4.2059	-12.5339	-1.9948
1000.	-1.2250	-.0517	-1.7809	-1.3700	-8.5243	-3.9689	-11.8947	-1.9438
1050.	-1.2611	-.0540	-1.7239	-1.2829	-8.3153	-3.7482	-11.2962	-1.9011
1100.	-1.3009	-.0567	-1.6670	-1.2053	-8.1143	-3.5428	-10.7345	-1.8668
1150.	-1.3444	-.0597	-1.6115	-1.1360	-7.9220	-3.3521	-10.2065	-1.8410
1200.	-1.3911	-.0630	-1.5580	-1.0738	-7.7385	-3.1750	-9.7093	-1.8235
1250.	-1.4403	-.0666	-1.5072	-1.0180	-7.5641	-3.0108	-9.2403	-1.8141

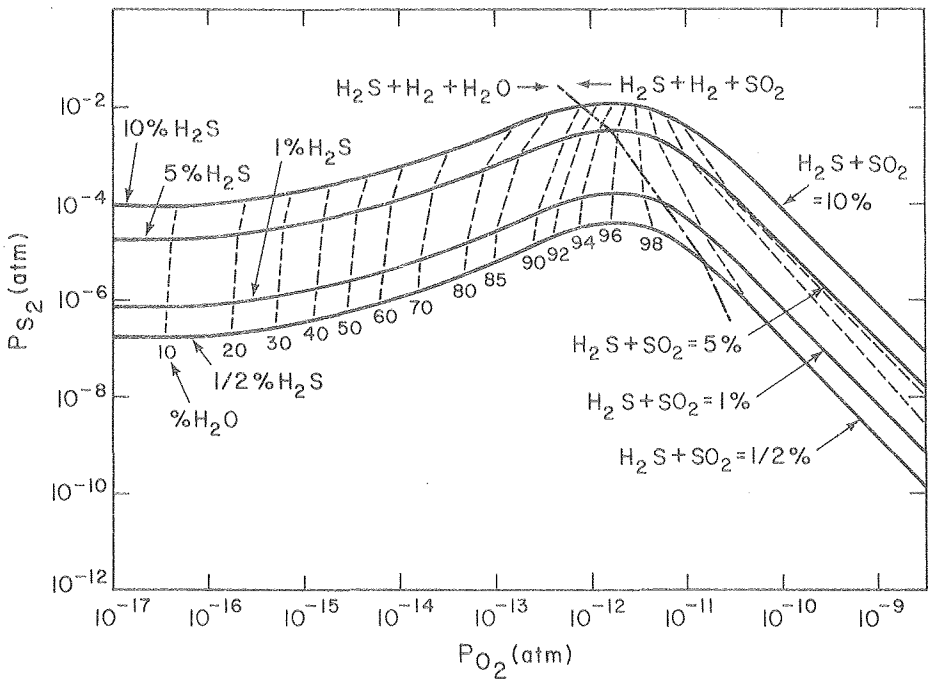

Fig. 1. Sulfur potential as a function of oxygen potential in equilibrated gas mixtures in the S-O-H system. (XBL 802-262)

lies close to the co-existence line for NiS and NiO, and as a consequence this interdependency between sulfur and oxygen potentials is much more critical for Ni-base materials. In other systems the maximum in the sulfur/oxygen potential curve lies to the right of the sulfide/oxide stability line and it is unlikely that localized fluctuations in gas composition can ever shift the gas into a purely sulfide forming regime, although sulfides may form via other mechanisms.

* * *

2. CORROSION MECHANISMS IN COMPLEX ENVIRONMENTS OF LOW OXIDIZING POTENTIAL

I. M. Allam and D. P. Whittle

Pure Fe. Competitive formation of oxides and sulfides in environments that can sustain the formation of either or both phases has been studied in an attempt to establish the critical parameters which control the overall corrosion process. Pure iron samples were exposed to H_2O-H_2-H_2S mixtures of various compositions introduced into the test rig through metered flows. A constant sulfur fugacity, 8.4×10^{-6} atm, was used for most of the experiments while the oxygen fugacity was varied over the range in which sulfide or oxide is the more stable phase.

Figure 1 shows a stability diagram for the Fe-S-O system with the gaseous environments included. At a $PO_2 = 3.2 \times 10^{-12}$ atm (point A), which is inside the Fe_3O_4 stability region, no sulfidation occurs and the growth rate of the FeO is independent of the presence of sulfur in the environment. The reaction path lies totally within the oxide region and this is related to the low solubility of sulfur in the Fe_3O_4 phase formed at the surface. When the PO_2 is reduced, 3.3×10^{-13} atm (point B), FeO is now in contact with the gas. It is possible that this phase has a higher solubility for sulfur than does magnetite and that sulfur can transport through the oxide giving rise to sulfide formation throughout the oxide layer and beneath it as shown in the scale cross-section in Fig. 2. However, a more consistent explanation relates to the location of the sulfide phase in the oxide scale: the sulfide is the lighter-colored phase appearing as globules within pores in the FeO and as continuous films, along the columnar grain boundaries of FeO. These boundaries, where they are in contact with the gas, represent deep cavities in which stagnant pockets of gas can collect. Further formation of oxide at these locations reduces the oxygen potential (or H_2O content) to the point where sulfide is the stable phase. Inclusion of the reactive gas in closing pores has the same effect. This continuous film of sulfide provides a path through which the sulfur is transported down through the oxide scale. The sulfide is liquid at this temperature. Indeed, at the base of the oxide scale the FeS interacts with both oxide and metal, forming an even lower melting point (925°C) liquid, which on post-exposure examination solidifies as a FeS-Fe-FeO eutectic: phase relationships in the Fe-O-S system are more complex than implied in Fig. 1 and need to be determined.

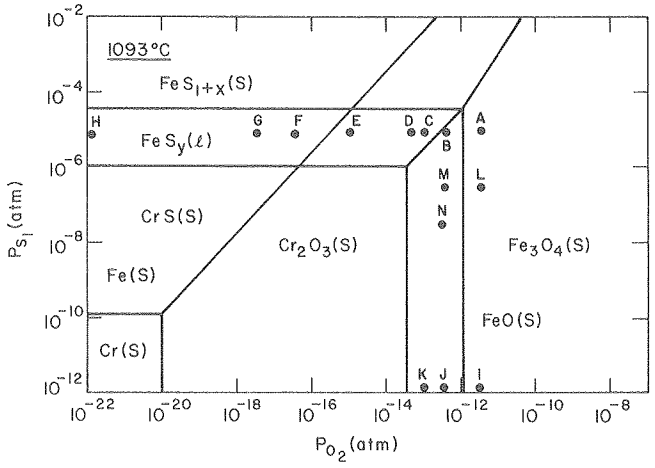

Fig. 1. Thermodynamic stability diagram of the Fe-S-O and Cr-S-O systems at 1093°C showing gaseous compositions. (XBL 802-272)

Changes in the oxide to sulfide ratio in the scale occur when the bulk H_2O content of the gas is lowered ($PO_2 = 1.0 \times 10^{-13}$ atm, point C, Fig. 1) and the gas mixture moves into a region where the sulfide should be stable in contact with the gas. Mixed sulfide and oxide protrusions grow outwards from the surface scale (Fig. 3) which is again consistent with a gaseous transport step being an important part of the overall growth process.

This is further substantiated by other observations. Variation in the volume flow rate of the reactive gas mixture produces two effects: (i) there is a marked change in the scale growth rate, and (ii) there is a change in the relative amounts

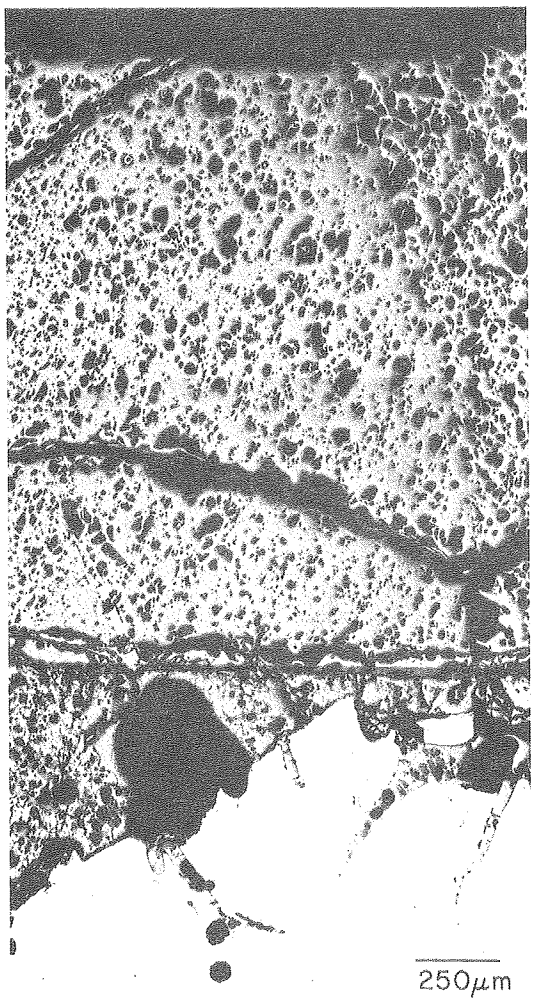

Fig. 2. Cross section of scale formed at gas composition B after 24 hr exposure. Note presence of globules of light-colored FeS phase associated with pores in oxide scale, and as continuous films at columnar grain boundaries. (XBB 802-2445)

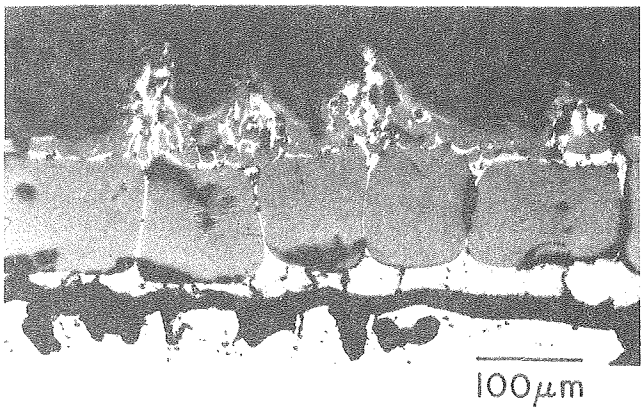

Fig. 3. Cross section of scale formed at gas composition C after 2 hr exposure. Note oxide/sulfide protrusions on outer surface of scale above columnar grain boundaries and layer of sulfide beneath oxide. (XBB 802-2443)

of sulfide and oxide formed. Increase in the flow rate from 200 cc/min, the condition producing the scale shown in Fig. 2, to 800 and 1200 cc/min produced scale thicknesses in 2h exposure of 350 and 810 μm respectively in comparison with 110 μm at the lower flow rate. The amount of sulfide formed decreased also, and was virtually nonexistant at the highest flow rate. In contrast, decrease of the flow rate to 50 cc/min produced a scale consisting essentially of only the liquid FeS-FeO phase, and virtually no FeO as a separate phase. This scale was only 10 μm after 2h, but this low figure may be somewhat misleading, since the liquid scale tends to run off the surface. With further decrease of the PO_2 (5.2×10^{-14} atm, point D), FeO disappears as a separate phase in the scale, and only the FeS-FeO liquid is formed. At still lower PO_2 (3.2×10^{-17} atm, point E), below the stability limit of FeO, the liquid scale is only FeS. The compositions of the liquid scales are not dependent on the gaseous flow rate: the liquid phase is not able to sustain crevices or pores at its growing surface.

Cr_2O_3 - Forming Alloys. Cr_2O_3 is considered to be among the best protective barriers for oxidation resistance. It is thermodynamically very stable (see Fig. 1), and grows slowly due to its low concentration of native defects. Whether it can remain as a protective barrier for Fe-base alloys in the presence of sulfur in the gas phase needs to be established, and has been investigated by exposing binary Fe-Cr alloys to H_2-H_2O-H_2S mixtures as outlined above. Generally, lower oxygen potentials were used, corresponding to conditions where Cr_2O_3 and FeS can be in equilibrium with the gas: these are marked in Fig. 1.

The thickness of the Cr_2O_3 grown at a $PO_2 = 1 \times 10^{-5}$ atm and $PS_2 = 8.4 \times 10^{-6}$ atm (point E) depends on the Cr content of the alloy, being 10, 20, 25, and 30 μm in 100h exposure on Fe-18, 25, 40% Cr and pure Cr respectively. In addition, on pure Cr, small, discrete particles of CrS form beneath the surface oxide, and to a lesser extent on Fe-40% Cr and pure Cr, but not with the more dilute alloys. Interestingly, the morphology of the oxide changes from an apparently porous outer structure, to a very compact layer close to the metal interface. Calculations indicate that the diffusion rate of chromium in the alloy is sufficiently large that the flux of chromium out of the alloy is not a rate-limiting step, although a depletion of Cr does exist in the alloy behind the growing Cr_2O_3 scale. Instead, the oxygen potential gradient, and in turn the defect gradient, is influenced by the Cr concentration at the alloy surface, more so than when Cr_2O_3 grows in pure O_2 containing environments where the defect gradient is largely influenced by the conditions at the outer oxide/gas interface. The decrease in the defect gradient upon reducing the Cr content of the alloy, reduces the growth rate of the oxide, but more importantly reduces the inward diffusion of sulfur. The diffusion path cuts through the sulfide region for pure Cr and alloys rich in Cr, but remains in the oxide phase field. This cannot be shown on a two-dimensional stability diagram, such as Fig. 1, and diagrams with alloy composition as a third axis are required.

As the oxygen potential is reduced (point G in Fig. 1), the diffusion path cuts into the CrS region independently of the Cr content of the alloy, and CrS is formed as a separate phase beneath the Cr_2O_3 in all cases. Figure 4 shows a typical cross section. The overall consumption rate of Cr from the alloy is now somewhat higher and the Fe in the alloy cannot back diffuse into the alloy at a fast enough rate and is included into the growing scale as unoxidized metal, as indicated in the x-ray maps of Fig. 4. Note that the Fe forms neither a sulfide nor an oxide, and this is related quantitatively to the position of the diffusion path on the Fe-Cr-S-O stability diagram. Quantitative evaluation of the diffusion path is hindered by the lack of transport data in the Cr-rich sulfide and oxide phases.

Another feature of the behavior of these alloys relates to the formation of liquid iron-rich sulfides at some locations on the samples. These cannot have formed via a diffusional process and are related to a loss of adhesion of the Cr_2O_3, exposing the now Cr-denuded alloy to the sulfur-rich gas. As such, this breakdown is more prevalent near corners of the samples and the iron sulfide-rich liquid spreads out over the surface surrounding Cr_2O_3 scale seemingly without interacting further.

When the oxygen potential is reduced to 3.3×10^{-18} atms (point H), CrS becomes the stable phase in equilibrium with the gas, but the reaction path cuts into the Cr_2O_3 region. This reaction path is independent of the Cr content in the alloy. The scale thickness, however, increases from 250-300 μm for Fe-18Cr to 425-450 μm for Fe-40Cu and ~850 μm for pure Cr. Except for the case of pure Cr, a CrS subscale forms within the alloy beneath the Cr_2O_3 that develops at the metal surface. The outer Cr scale contains substantial amounts of Fe, dissolved in solid solution.

Thus, the results show that two types of sulfur-induced degradation seem possible in these low oxygen potential atmospheres: the one is related to transport of sulfur through the Cr_2O_3 scale, and the other to a complete mechanical loss of the protective oxide.

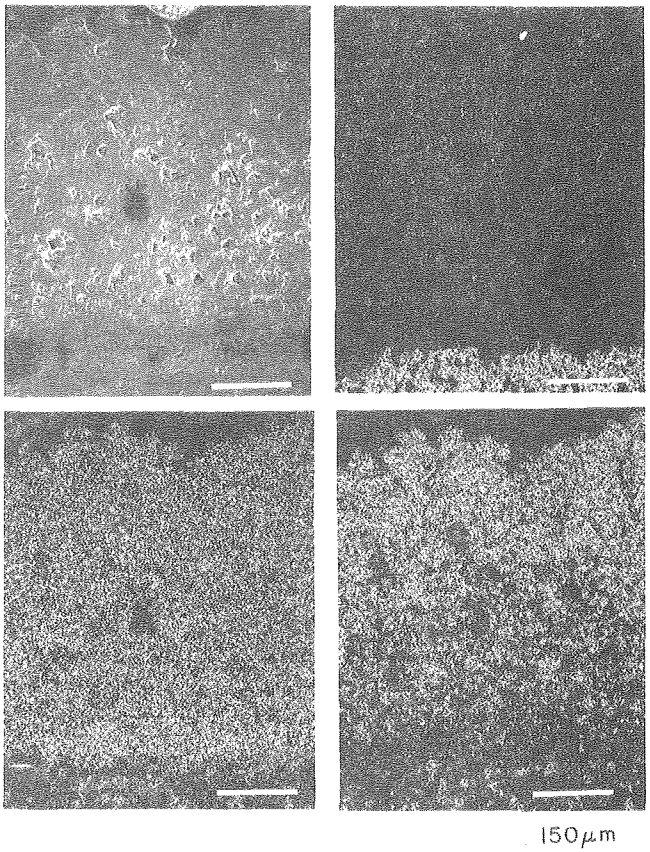

Fig. 4. Cross section of the scale formed at gas composition G after 190 hr exposure. Note Fe rich particle embedded in CrS protrusion below a Cr_2O_3 scale. (XBB 802-2446)

* * *

3. HOT CORROSION OF NICKEL-BASE ALLOYS AT INTERMEDIATE TEMPERATURES†

A. K. Misra and D. P. Whittle

It is now reasonably well established that there are two quite distinct types of hot corrosion involved in the degradation of turbine blading materials. Type I occurs at temperatures above 900°C and is caused by the deposition of molten Na_2SO_4 on the blades in air turbines. Type II occurs at somewhat lower temperatures, 700-850°C, and is more prevalent in marine and industrial turbines. Type II is also caused by sulfatic deposits. These are low melting point eutectics formed between the solid Na_2SO_4 deposit and $NiSO_4$ or $CaSO_4$, formed by sulfation of NiO and CoO, the corrosion products of typical alloys. Propagation of type II corrosion, then, is dependent on a liquid sulfate being formed and the presence of significant, though small, concentrations of SO_3 in the gas phase. This project is aimed at identifying the factors controlling type II hot corrosion, and establishing mechanisms.

Ni-base Cr_2O_3 - forming alloys seem to be the most resistant to attack when coated with Na_2SO_4 in Na_2SO_4-$NiSO_4$ eutectic mixtures and exposed at 750°C to air containing 1.5×10^{-3} SO_3. Transport of the oxidant across the molten salt is a critical factor, and evidence points to oxygen diffusivities being very low; SO_3 may, however, transport as a pyrosulfate, $S_2O_7^=$ ion, and it has been shown that the continued propagation of the hot corrosion is via a sulfidation/oxidation mechanism. Dissolution or fluxing of Cr_2O_3 by the melt is not observed.

Al-containing alloys are very heavily corroded by the salt films, even Ni-25Cr-2.5Al which is still a Cr_2O_3 - forming alloy. Figure 1 shows a section through a sample coated with 2 mg/cm^2 Na_2SO_4 and oxidized in air + 1.5×10^{-3} SO_3 for 15h at 750°C. The scale has a pronounced banded structure with alternate layers of Cr- and Ni-rich phases. This is typical of a fluxing type of process and it is clear that Al_2O_3 dissolves in the Na_2SO_4 -$NiSO_4$ melt, probably as its sulfate. Thermodynamically, sulfation of Al_2O_3 would not be expected at the prevailing SO_3 partial pressure; however, the activity of $Al_2(SO_4)_3$ in the melt is probably quite low, promoting the reaction. The solution behavior of ternary sulfate melts of this type are not known.

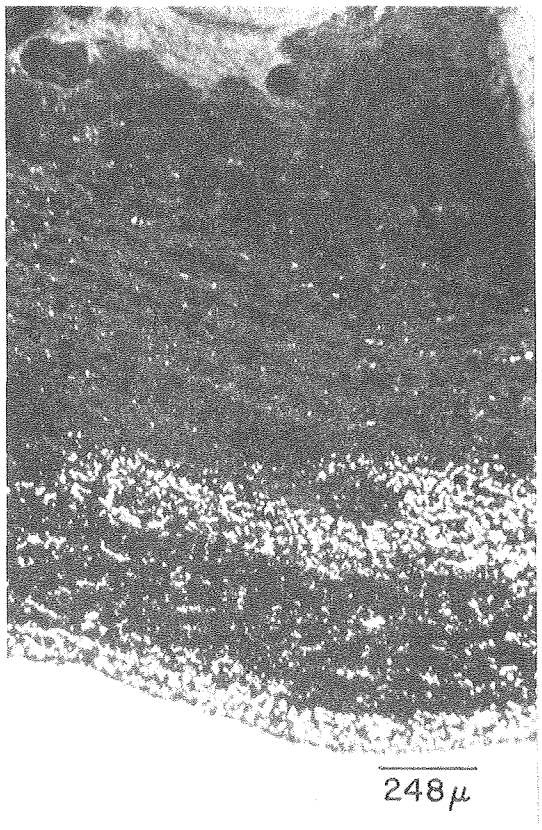

Fig. 1. Cross section of Ni-25Cr-2.5Al coated with 2 mg/cm^2 Na_2SO_4 and oxidized in air + 1.5×10^{-3} SO_3 for 15 hr at 750°C. (XBB 7910-13488A)

* * *

†Brief version of paper presented at Electrochem. Soc. Meeting, Los Angeles, California, October 1979.

4. CORROSION BY SOLID SULFATIC DEPOSITS†

H. C. Akuezue and D. P. Whittle

Fluidized bed combustion, although not a new concept, provides a novel process for burning a wide range of fuels efficiently at high combustion intensities, while keeping the emission of sulfur and nitrogen oxides well below any of the rigid standards currently being proposed or in force. Coal and suitably sized sorbent particles are introduced to the combustor where combustion of the coal occurs. The coal combusts at a relatively low temperature, in the range 750-950°C, which enables good sulfur retention by the sorbent in the bed; this temperature is also below the ash fusion point. Limestone or dolomite are the preferred sorbents: they react with the SO_2 released during combustion to form calcium or magnesium sulfates. Originally it was anticipated that fireside corrosion problems of in-bed steam-raising tubes by the ash/coal/calcium sulfate burden would be minimal; however, tests have shown that a severe sulfidation/oxidation type attack can occur even though most of the agressive sulfur compounds that could have accounted for the sulfidation have reacted with the acceptor. The generation of sulfur activities sufficiently high to sulfidize the alloys implies that the oxygen potential of the system, at least locally, is relatively low, since the two potentials are related through the CaO/CaS/$CaSO_4$ equilibria. This study, then, examines the behavior of typical Cr_2O_3 - forming alloys in the presence of $CaSO_4$/CaO mixtures in atmospheres of controlled oxygen potential, in the range 10^{-19} -1 atm, using CO/CO_2 mixtures.

The corrosion rate at a constant temperature, 850°C typical of operational temperatures, increased with increasing oxygen activity, and furthermore there was no sulfidation. This is contrary to the earlier expectation that the $CaSO_4$ - induced attack should depend only on the sulfur activity according to the Ca-O-S stability diagram. Interaction between the $CaSO_4$ and the oxides of iron which form on top of the protective Cr_2O_3 scale was responsible for the accelerated attack. $CaFeO_2$ was formed, which had a cubic structure with unit cell length of 4.726 Å and a composition of 72.6% CaO, 22.0% FeO and 4.9% Fe_2O_3. Direct observation of this interaction in the hot stage SEM indicated that the $CaFeO_2$ phase appeared to melt at around 927°C. Indeed, temperature was far more important than the oxygen potential in inducing sulfidation attack. Figure 1 shows a section through the scale formed on IN800 (Fe-32%Ni-20.5%Cr-0.35%Si-0.75Mn-0.04%C-0.3%Cu) exposed to $CaSO_4$ containing C at 950°C in a static air environment. Heavy internal sulfidation occurs with the precipitation of Cr-rich sulfides within the alloy, primarily at grain boundaries. This concentrates the chromium in the grain boundaries and prevents the establishment of a continuous Cr_2O_3 protective layer. Once sulfides have been introduced into the alloy they continue to penetrate further by being oxidized at the alloy/state interface, with the released sulfur diffusing further into the alloy.

There appear to be two aspects of $CaSO_4$ - induced attack: (a) At low temperatures, below 950°C, a direct reaction between the oxide scales and $CaSO_4$ that does not involve sulfidation. In iron-base

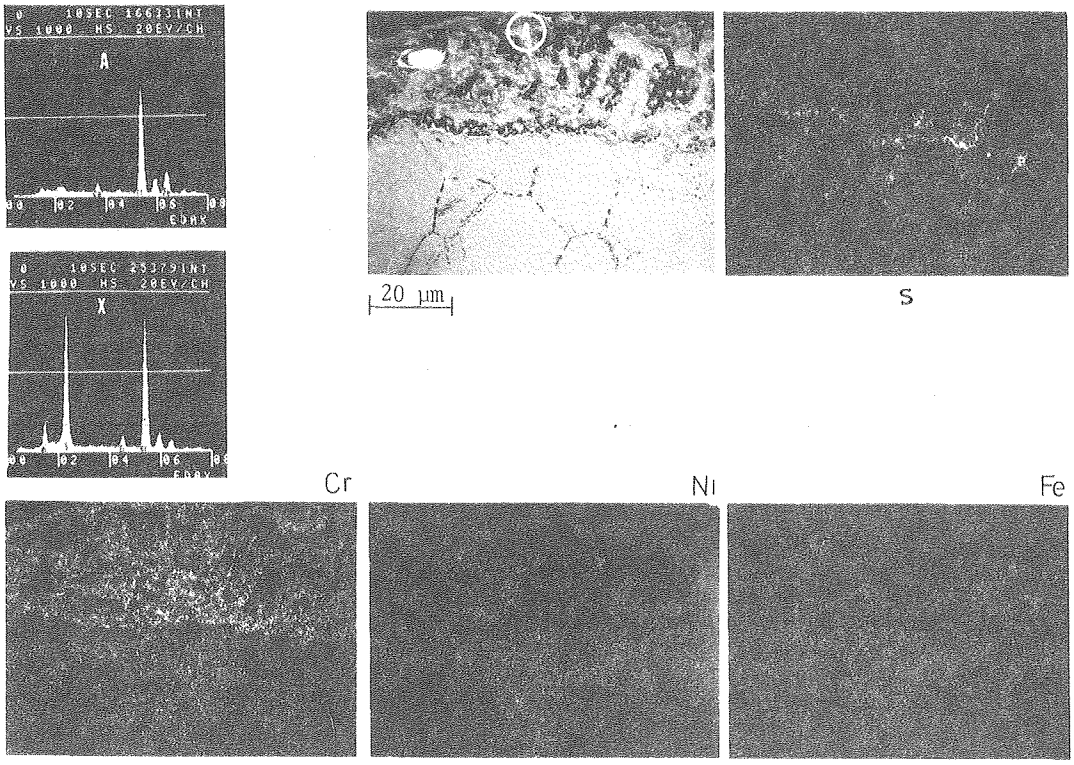

Fig. 1. Scanning electron image, x-ray maps and EDAX analyses of the cross section of the scale formed on alloy IN800 exposed to $CaSO_4$ + C deposit for 100 hr at 950°C in static air. (XBB 790-15069)

materials, the main scale contains nonprotective, porous $CaFe_2O_4$ spinel, and the outermost scale is a thin, sometimes loosely adhering complex calcium-iron sulfate. (b) A complex calcium-iron sulfate liquid phase attack that occurs at high temperature, above 950°C, and induces an oxidation/sulfidation attack that is catastrophic.

* * *

†Brief version of LBL-10286.

5. ADHERENCE OF Al_2O_3 OXIDE FILMS†

H. C. Akuezue, I. M. Allam, and D. P. Whittle

Adhesion between surface scale and alloy substrate is essential for good oxidation resistance. Poor adhesion can lead either to exfoliation of the oxide in response to thermal cycling, or to mechanically applied stresses, resulting in enhanced oxidation rates. Marked improvements in scale/substrate adhesion, however, can be achieved via the "rare-earth effect" whereby addition of a small amount of a rare-earth element or of a fine distribution of a stable oxide produces a significant increase in an alloy's resistance to cyclic oxidation. Recent work[1] has demonstrated that the major factor responsible for the improved scale adherence with Al_2O_3 - forming alloys is the formation of protrusions of oxide growing into the alloy. These act to key the protective scale to the surface and are more effective when a uniform distribution of small oxide pegs can be achieved at the alloy/scale interface. This is difficult to control with metallic additions since essentially the active element oxidizes internally during high temperature exposure, and these internally precipitated oxides form the nuclei around which the protective oxide forms the pegs. Clearly, the distribution of the internal oxides, and hence the subsequent pegs, depends on the exposure conditions and is thus not directly controllable.

Several reports have indicated that marked improvements in Al_2O_3 scale adherence are also achieved by the presence of Pt in the alloy, and it seemed possible that the formation of the intermetallic $PtAl_3$ might be involved, and that this might exist as a fine dispersion in the alloy which acted in the same way as an oxide dispersion. $PtAl_3$ is very stable, although its formation might reduce the affective Al content of the matrix. However, Pt and Hf additions could be made together, and the intermetallic $HfPt_3$ used as the dispersoid. This is even more stable, does not contain Al, and, if it did oxidize, would produce an HfO_2 - oxide dispersion anyway.

The principal alloy studied was Co-10Cr-11Al (wt.%), which forms an external scale of α-Al_2O_3 over the temperature range studied. Additions of 1 Pt, 1 Hf-3Pt or 0.3Hf-0.9Pt (all wt.%) were made to this base alloy. Oxidation experiments were of two types: (a) isothermal exposure, and (b) repeated thermal cycles of 20hr duration each. The detailed morphology of the alloy/scale interface was studied by stripping the scale and examining its underside and, when possible, the exposed surface of the alloy. Scales were stripped either mechanically by quenching in liquid nitrogen, or with particularly adherent scales, the substrate was dissolved away using a 10% bromine in methanol solution.

The alloy microstructures are very similar and consist principally of a dark, dendritic, β-CoAl phase in a lighter, α-Co matrix. There is also a third, very dark precipitate phase identified by EPMA as the Hf-Pt-rich intermetallic which appears to be confined to the α-Co matrix.

Both Pt and Pt+Hf reduce the oxidation rate of the Co-10Cr-11Al alloy under isothermal conditions at 1100°C. Under cyclic oxidation conditions, Pt additions alone have little effect, but the 0.3Hf + 0.9Pt addition significantly improves the oxidation resistance. The alloy containing 1Hf + 3Pt shows a lower resistance. Weight gain/time curves are shown in Fig. 1.

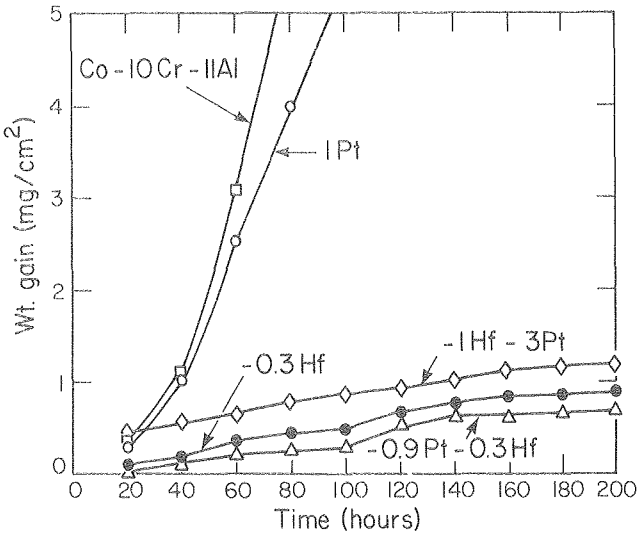

Fig. 1. Weight gain/time data for the cyclic oxidation of Co-10Cr-11Al alloys containing Pt and/or Hf at 1100°C. (XBL 798-2391)

The Al_2O_3 scale which formed on the alloy Co-10Cr-11Al-1Pt after 265 h oxidation at 1200°C was not adherent and spalled from the alloy on cooling. Similar features were observed with the ternary Co-Cr-Al alloy of the same composition oxidized under similar conditions.

Surface examination of the alloy Co-10Cr-11Al-0.3Hf-0.9Pt after oxidation at 1200°C indicated that the scale was tightly adherent to the substrate and spalled during cooling only from very small discrete areas. The major difference between this alloy and an alloy that was Pt-free but containing Hf[1] was that with the Pt-free alloy, the substrate surface appeared to be more heavily convoluted.

Figure 2 shows the underside of the Al_2O_3 scale after the alloy substrate has been dissolved away. This is the Co-10Cr-11Al-1Hf-3Pt alloy, oxidized isothermally for 200hr at 1100°C. This regular distribution of oxide protrusions compares well with those obtained in previous studies.[1] The protrusions do not penetrate so deeply and are not as tortuous in shape as those formed in the case of a Co-10Cr-11Al-0.3Hf alloy, but compare well with those formed when this latter alloy had been given a pre-internal oxidation treatment prior to exposure. This regular distribution of oxide protrusions is the most desirable in determining oxide/scale adherence. EPMA indicates that the pegs consist primarily of Al_2O_3, encapsulating the dispersed phase. Presumably they grow by some form of short-circuit diffusion of oxygen along the incoherent interface between the matrix and the dispersiod. As a consequence the composition of the dispersed phase is not critical.

The average spacings between the Al_2O_3 pegs and those of the dispersion phase in the alloy are quite similar for each alloy and typically are 3-4 μm along the interface. The length of the peg protruding into the alloy is also important. Typically these are in the range 5-10 μm with the alloy containing 1Hf-3Pt and slightly less than this for the 0.3Hf-0.9Pt alloy. Long protrusions tend to promote scale cracking above the pegs.

Thus, the intermetallic dispersions of Hf and Pt formed in Co-10Cr-11Al alloys are comparable in size and distribution to the HfO_2 dispersions produced by pre-internally oxidizing Co-10Cr-11Al-Hf alloys and seem to provide an alternative way of producing a dispersed phase in these alloys. This opens up the possibility of exploring other dispersion-containing metallic systems. The inwardly growing Al_2O_3 pegs which develop on subsequent exposure to oxidizing environments seem equally effective in keying the Al_2O_3 surface scale to the substrate and thereby improving the oxidation resistance of this type of alloy under both isothermal and particularly thermal cycling conditions.

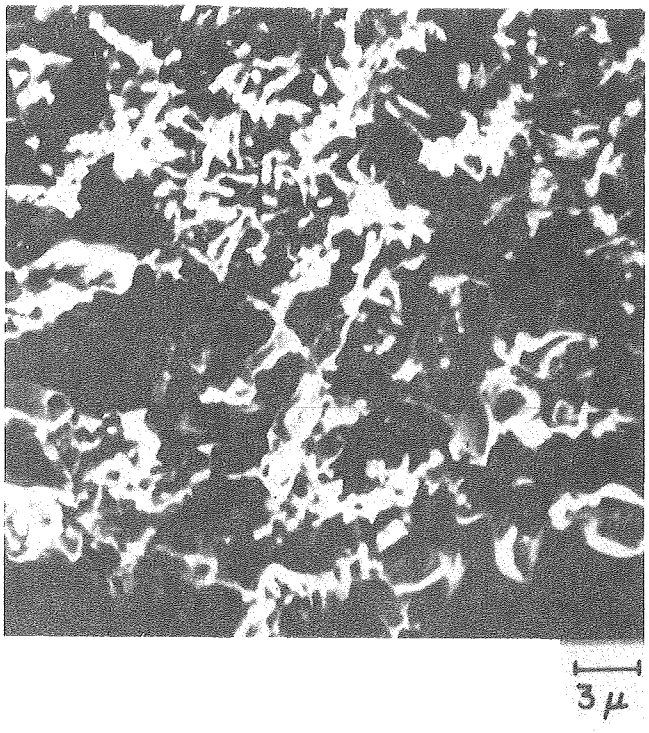

Fig. 2. Underside morphology of the Al_2O_3 formed on Co-10Cr-11Al-1Hf-3Pt after isothermal oxidation of 1100°C for 200 hr: alloy substrate has been dissolved away. (XBB 798-10392)

* * *

†Brief version of LBL-9180; accepted for publication in Oxid. Metals.

1. I. M. Allam, D. P. Whittle and J. Stringer, Oxid. Metals 12, 35 (1978); 13, 381 (1979).

6. OXIDATION BEHAVIOR OF A TWO-PHASE ALLOY: Fe - 44%Cu†

F. Gesmundo,‡ P. Vianni,‡ and D. P. Whittle

During the high-temperature oxidation of alloys the scales that form often contain a number of different phases, each of which may contain more than one alloy component. Thus, the ratio of the metals in the scale is different from this ratio in the alloy because the various components have different affinities for oxygen, and the rate of transport in the scale is different for each cation and in each phase. The composition of the scale may also vary with position due to these differening diffusivities. Some success has been achieved in attempts to correlate the theories of alloy oxidation kinetics with diffusional, structural and compositional parameters of the metal oxides in systems in which a solid solution scale is formed. Here that theme is continued in attempting to analyze the behavior of systems in which the oxides of the constituent metals are virtually immiscible, and the overall oxidation rate depends heavily on the distribution of the various oxide phases in the scale. In addition, Fe and Cu are relatively immiscible in the metallic phase, and large compositional changes in the alloy due to preferential oxidation are therefore precluded even though there are considerable differences in stabilities between iron and copper oxides.

The microstructure of the alloy after annealing consists essentially of the as-cast, dendritic structure. The dendrites are the iron-rich phase which, according to the phase diagram, contains 5.81 wt% Cu; the copper-rich matrix contains 2.06 wt% Fe at 1000°C. The average size of the iron-rich phase particles is around 20-30 μm.

The isothermal oxidation rate follows, to a good approximation, a parabolic law, and the rate constants (g^2 cm^{-4} s^{-1}) as functions of temperature are reported in Table 1. Comparison of the alloy oxidation kinetic constants with those of the pure base metals shows an improved resistance of the alloy to oxidation; the alloy oxidizes marginally more slowly than pure copper, but substantially more slowly than iron. The ratio between alloy and pure copper parabolic rate constants remains almost constant up to 900°C and then decreases sharply, whereas for a similar ratio between alloy

Table 1. Comparison of parabolic rate constants for oxidation of Fe-44% Cu with pure Fe and pure Cu. [Data for Cu are from D. W. Bridges et al., J. Electrochem. Soc. 103, 475 (1956) and S.Mrowee and A. Stocklosa, Oxid. Met. 3, 291 (1971); those for Fe are from M. H. Davies et al., Trans. AIME 191, 889 (1951)].

	Parabolic rate constants ($g^2\ cm^{-4}\ s^{-1}$)				
$T_{(°C)}$	Cu	Fe	Alloy	$\frac{k_{Cu}}{k_{all.}}$	$\frac{k_{Fe}}{k_{all.}}$
700	1.72×10^{-9}	6.0×10^{-9}	$2.61 \pm 0.06 \times 10^{-10}$	6.6	23
800	5.53×10^{-9}	5.7×10^{-8}	$8.61 \pm 0.85 \times 10^{-10}$	6.4	66
900	2.80×10^{-8}	2.5×10^{-7}	$4.73 \pm 0.001 \times 10^{-9}$	5.9	53
1000	8.1×10^{-8}	$\sim 1.1 \times 10^{-6}$	$3.11 \pm 0.03 \times 10^{-8}$	2.6	35

and iron a maximum is observed at 800°C. There are four principal scale layers as shown in Fig. 1: an outer CuO, a layer of $CuFeO_2$ or magnetite layer, and an inner wüstite layer. In addition, there is a form of internal oxidation of the Fe-islands within the alloy. After longer oxidation times, the outer CuO layer develops considerable porosity, which tends to be elongated in the growth direction. The amount of Fe dissolved in this layer is about 7 wt% and the Cu concentration in the inner layers is 3.5 and 1.0 wt% in Fe_3O_4 respectively, at least for samples exposed at 900°C. Significantly less intersolubility between the component oxides is observed at lower temperatures.

The main reason for the reduced oxidation rate of this alloy in comparison with pure Fe, is the reduced relative thickness of the inner FeO layer. Generally, on iron this phase constitutes about 95% of the total oxide scale formed in the temperature range 700-1200°C. In the case of the alloy, the oxygen activity at the alloy/scale interface is higher, since it can be noted that the iron-rich phase of the alloy is oxidized to FeO and the only remaining metal phase is the Cu-rich ε-phase. In the saturated ε-phase the Fe activity is as high as 0.9486 even though its atomic fraction is only 0.0234, so that the activity coefficient, γ°, assuming Henry's law, is 40.54. A lower limit for the Fe concentration in the ε-phase is equilibrium with FeO corresponding to an oxygen activity equal to that between FeO and Fe_3O_4. Using free energy data, this minimum Fe activity is 0.1284 with the corresponding atomic fraction of 0.0032. The growth rate for the direct formation of magnetite on an iron alloy having this metal activity then has been calculated from transport rates in Fe_3O_4, giving 3.5×10^{-10}, 2.5×10^{-9}, 1.3×10^{-8} and 5.1×10^{-8} $g^2\ cm^{-4} s^{-1}$ at 700, 800, 900 and 1000°C respectively. These are somewhat larger than the measured values, and the pressure of Cu_2O as an outer layer may have reduced the oxygen activity at the outer interface of the magnetite layer, which would reduce the growth rate further. An additional contribution to the observed decrease in the scaling rate may also arise from the dissolution of Cu in the Fe oxides. In fact FeO, in spite of its large deviation from stoichiometry and the complex nature of its defects, is essentially a p-type semiconductor, so that the presence of copper--most probably in the form of Cu^+ ions, owing to the low oxygen activity--should produce a decrease in the vacancy concentration and hence slow down the diffusion of iron. Actually, large additions would be thought necessary for this effect, due to the high concentration of native defects in FeO as compared to similar oxides like NiO or CoO.

Possible stress effects associated with the development of different oxides growing at different rates on the alloy seem to be absent from this system. In fact, the scale appears compact and of uniform thickness and shows no lateral variations in structure or composition, at least none which can be directly associated with the two-phase structure of the alloy only. The thickness of the wüstite layer sometimes shows large variations around the surface of the sample, where at some positions it is confined to the internal oxidation region, while in others it extends far into the scale. The relative uniformity of the scale structure is possibly related to the small grain size of the alloy, so that Cu-rich and Fe-rich regions in the alloy alternate frequently at the alloy/oxide interface and lateral diffusion is sufficiently rapid to even out these fluctuations: differences in the scale structure are in fact confined mainly in a direction perpendicular to the alloy surface rather than parallel to it.

* * *

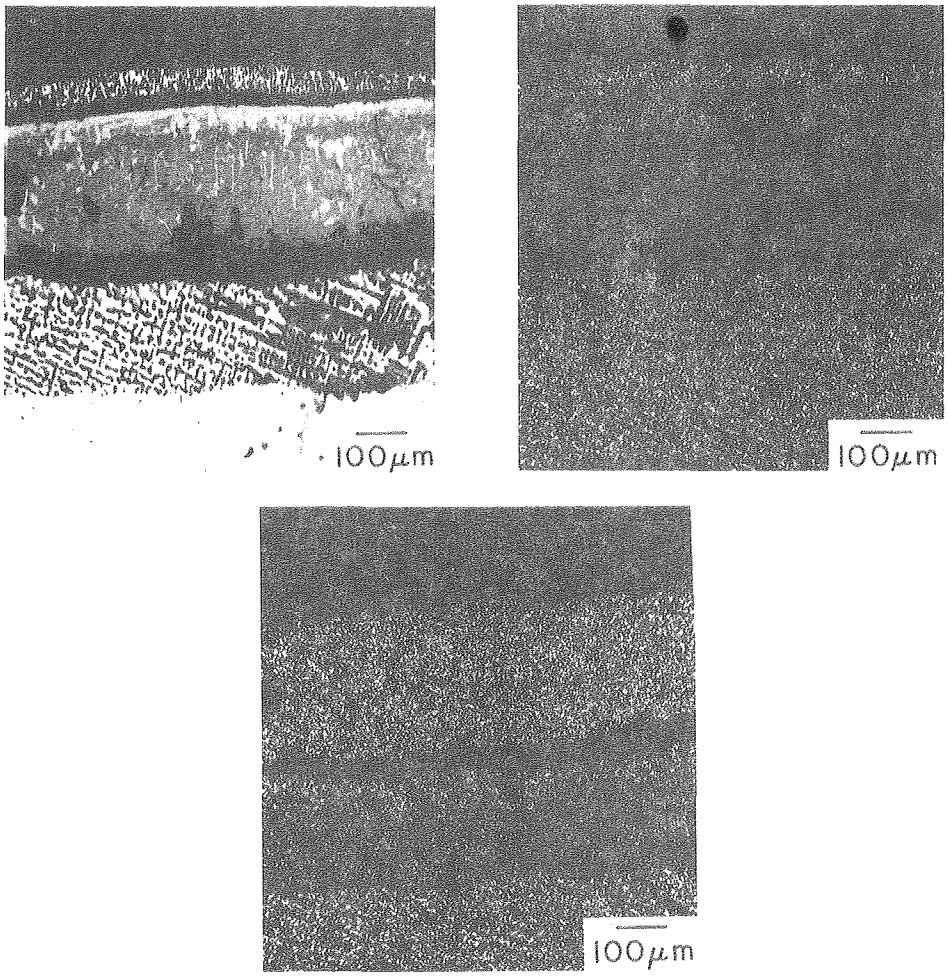

Fig. 1. Cross section of the oxide scale formed on Fe-44% Cu oxidized for 6 hr at 900°C in air. (XBB 802-2444)

* * *

†Brief version of LBL-10452; to be published in J. Electrochem. Soc.
‡Centro Studi di Chimica e Chimica Fisica Applicata, Consiglio Nazionale delle Ricerche, Genoa, Italy.

7. FORMATION OF SUBSCALES OF VARYING COMPOSITION†

D. P. Whittle, F. Gesmundo,‡ B. D. Bastow,§ and G. C. Wood‖

Significant progress has been made recently[1] in the quantitative analysis of alloy oxidation phenomena, particularly in systems where a single phase scale, but containing both alloy components, is formed. This model, however, ignores the possibility of forming a subscale within the alloy beneath the surface scale and although this does not affect the validity of the original treatment in any way, a full description of the scaling characteristics of this type of alloy requires analysis of the internal oxidation process also.

Internal oxidation in these systems, where both alloy components can and do enter the oxide phase forming an oxide solid solution, is somewhat different from that classically observed in other systems. The internally precipitated oxide is the same phase as the surface scale, and within the zone of internal oxidation, the fraction of internal oxide precipitated varies with position. Typical systems to which the analysis applies include binary alloys of Co, Fe, Mn and Ni with each other since the isotypic oxides CoO, FeO, MnO and NiO all have a simple cubic NaCl structure and form solid solutions over their entire composition ranges. Equally, the analysis is well suited to internal carbide precipitation when alloys are exposed to miscible. Degradation by internal carburization is rapidly increasing in significance in many studies relating to materials performance in coal conversion and petrochemical processing systems.

Figure 1 shows schematically a typical isothermal section of the alloy-oxygen phase diagram. The alloy and oxide systems referred to above approximate to thermodynamically ideal behavior, which simplifies the analysis, but does not limit its applicability. Included in Fig. 1 is the diffusion path which represents the locus of compositions through the alloy, subscale, and surface scale system. Portion ab represents the alloy behind the subscale zone, portions bc and de the compositions of alloy and oxide precipitates within the subscale region, with bd being the composite path in the subscale zone and indicating the relative fractions of the two phases, alloy and oxide. There is no overall change in composition in the subscale region, or in the alloy behind it, since the diffusivity of the interstitial oxygen within the alloy is far greater than that of the substitutional alloying elements. By the same token the average composition of metallic components in the oxide scale is identical to that in the alloy since the scale growth rate is orders of magnitude greater than interdiffusion in the alloy. There are concentration changes through the scale, ef, and these were calculated in the earlier paper.[1]

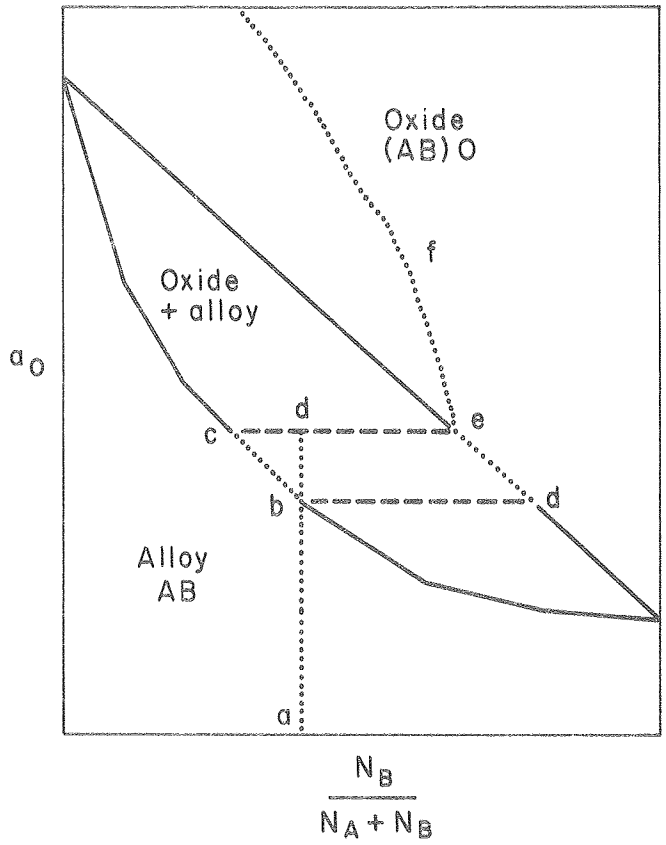

Fig. 1. Schematic phase diagram and diffusion path for the alloy-oxygen system. (XBL 802-317)

By expressing the amount of precipitated oxide as a function of alloy composition, using the phase diagram, the transport equation for oxygen in the subscale zone is modified to allow for the consumption of oxygen by precipitation and a transcendental equation for the penetration of the subscale front into the alloy obtained. Fraction of subscale, composition of the alloy and the composition of the subscale throughout the internal oxide zone can also be calculated.

Figure 2 shows the variation of the subscale/surface scale thickness ratio, ξ, with alloy composition, N_B^o, for different values of Ω and β which are the measures of the oxide stability: Ω is

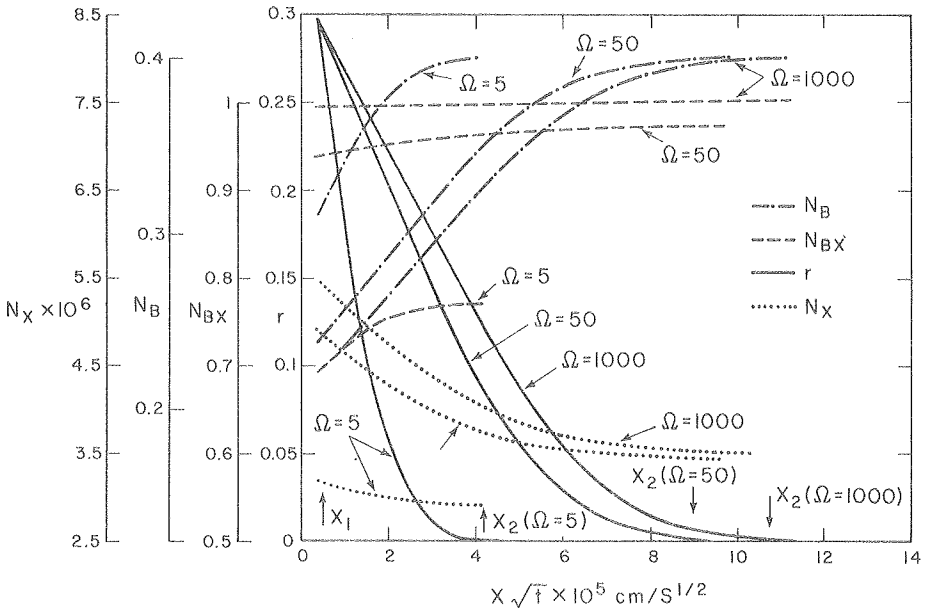

Fig. 2. Variation of internal oxide/surface oxide thickness as a junction of alloy composition and the stability of the oxide components. (XBL 802-320)

essentially the difference in stabilities of the two scale components and determines the slope of the boundary between oxide and oxide + alloy fields on the phase diagram. Increase in Ω, which increases the slope and corresponds to a greater difference in stability between the scale components, has a strong influence on the depth of subscale penetration. Increase in Ω also causes the maximum value of subscale/surface scale thickness ratio to occur at smaller values of N_B^o. β, which is a measure of the stability of the more stable scale component, has a lesser influence on the depth of subscale penetration. Its effect is opposite to that of Ω in that the larger the value of β, the smaller is the subscale penetration, and this is related to the lower overall solubility of the oxidant in the alloy. Other factors which affect the depth of subscale penetration include the diffusivity of oxygen in the alloy, and the rate of growth of the surface scale.

Swisher[2] measured the rate of internal oxidation of an Fe-1% Mn alloy exposed to a H_2O/H_2 mixture with $P_{H_2O}/P_{H_2} = 0.2$ at 1350°C obtaining a rate constant of 7.4×10^{-8} cm^2/s; the value calculated from our present analysis is 4.6×10^{-7} cm^2/s. However, as shown in Fig. 3 which expresses the variation of the fraction of internal oxide, the composition of the oxide and that of the alloy as a function of position within the internal oxidation zone, the fraction of internal oxide is only 0.012 at the surface of the alloy, its maximum value, and falls off rather rapidly through the internal oxide zone, decreasing to about 0.004 half-way across it. This means that it would be very difficult to observe the precipitation front with an optical microscope, and the measured value of the rate constant almost certainly represents an underestimation. Indeed, a better indication of the depth of internal oxidation can be obtained from Swisher's measurement of the Mn concentration profile: this gives a rate constant of 1.1×10^{-7} cm^2/s, somewhat closer to that given by the present analysis.

A better test of the analysis is to compare calculated and measured concentration profiles. The fraction of internal oxide particles or their composition have not been measured, but Fig. 3 compares calculated and measured Mn profiles. The agreement in shape and in absolute value is considered an acceptable test of the current analysis. The concentration profile calculated according to Swisher's analysis is also included; due to the assumptions made this has a physically unlikely discontinuity at the alloy/internal oxide interface

* * *

†Brief version of LBL-10067.
‡Centro Studi di Chimica e Chimica Fisica Applicata, Genova, Italy.
§British Nuclear Fuels, Windscale, Cumbria, UK.
‖Corrosion and Protection Center, U.M.I.S.T., Manchester, UK.

1. B. D. Bastow, D. P. Whittle and G. C. Wood, Proc. Roy. Soc. A356 177 (1977).
2. J. H. Swisher, TMS-AIME 242, 205 (1968).

RESEARCH PLANS FOR CALENDAR YEAR 1980

Studies of high temperature corrosion by gaseous environments containing sulfur and oxygen compounds will continue. Results to date have indicated that the buffering capacity of such gases, defined as the rate of change of sulfur potential with removal of oxygen, may be important, and this will be studied using gas mixtures in the S-O-H and C-O-S systems which have identical initial sulfur and oxygen potentials. Already it seems that the sulfur and oxygen potential of the gas are not necessarily the critical parameters in controlling behavior, and that the relative amounts of oxygen- and sulfur-containing species in the gas and the flow rate are involved. Studies will be extended to higher oxygen potentials where SO_2 is the major sulfidizing species. Transport through Cr_2O_3 has been shown to be critical and studies of the influence of dissolved sulfur on the defect chemistry and trasport properties of Cr_2O_3 are planned using thermogravimetric measurements in controlled atmospheres. Sulfur solubility as a function of sulfur

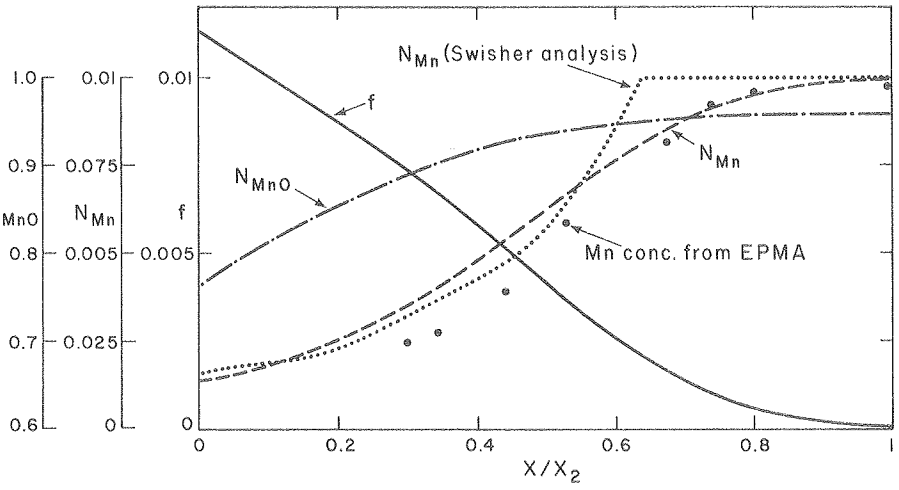

Fig. 3. Comparison of calculated and experimentally measured profiles for Fe-1% Mn oxidized in H_2O/H_2 (0.2) at 1350°C. (XBL 802-318)

and oxygen activity will also be determined. Attempts to construct meaningful alloy-O-S stability diagrams will be initiated, providing sufficient data exist.

Research into corrosion by liquid sulfate deposits has reached the stage at which the reactions of the sulfate melt should be studied in more detail. The formation of pertinent binary and ternary sulfates such as $NaAl(SO_4)_2$, $Na_3Cr(SO_4)_3$ and the $CoSO_4$ - $NiSO_4$ - Na_2SO_4 liquids as a function of SO_3 partial pressure will be studied. The mechanism of continued transport of SO_3 through the molten sulfate will be determined by SO_3 - solubility studies and Raman spectroscopy identification of the ionic state of sulfur compounds in the metal.

Oxide scale adhesion studies will be continued with attempts to develop a more quantitative description of the peg development at the alloy/scale interface. Low-angle erosion data will also be utilized as a potentially better method of quantifying scale adhesion. It is also planned to examine other parameters which can affect peg development: grain size, intermetallic and oxide dispersions, which can be varied more effectively by using actual PVD, sprayed and diffusion coatings. Microscopy studies of the early stages of oxide growth will also be initiated. A new program on the use of rare earth oxides added as surface deposited nitrates, to inhibit high temperature oxidation and scale spallation will be commenced.

Theoretical studies will concentrate on the growth of multiphase regions during diffusional-controlled reactions with particular reference to internal carburization as a degradation process. The ingression of interstitial elements such as oxygen and sulfur along alloy grain boundaries will be incorporated into the diffusion model.

1979 PUBLICATIONS AND REPORTS

Refereed Journals

1. D. P. Whittle and J. Stringer, "Improvements in High Temperature Oxidation Resistance by Additions of Reactive Elements or Oxide Dispersions," Phil. Trans. Roy. Soc. A27 (56), 209 (1979).

2. I. M. Allam, D. P. Whittle and J. Stringer, "Improvements in Oxidation Resistance by Dispersed Oxide Addition: Al_2O_3 - Forming Alloys," Oxidation of Metals 13, 381 (1979), LBL-9072.

3. O. T. Goncel, D. P. Whittle, and J. Stringer, "The Oxidation Behavior of Austenitic Fe-Cr-Ni Alloys Containing Dispersed Phases," Corros. Sci. 19, 305 (1979).

4. G. W. Roper and D. P. Whittle, "Interdiffusion in Ternary Co-Cr-Al Alloys," Metals Sci. J. (1980); LBL-8791.

5. F. Gesmundo, P. Nanni, and D. P. Whittle, "High Temperature Oxidation of Co-Mn Alloys," Corros. Sci. 19, 675 (1979).

Other Publications

1. D. P. Whittle, "General Aspects of High Temperature Corrosive Attack: Influence of Gaseous Atmosphere," High Temperature Corrosion, Commission of European Communities, Brussels (1979),

2. D. P. Whittle, "Hot Corrosion," High Temperature Corrosion, Commission of European Communities, Brussels (1979),

3. D. P. Whittle, "Introduction to Session on Corrosion," Proc. of Conf. on Corrosion/Erosion of Coal Conversion System Materials, Berkeley (1979), NACE, pp. 218-222.

4. K. N. Strafford, D. P. Whittle, P. J. Hunt and A. K. Misra, "The Corrosion of M-Cr-Al-Y-Type Alloys: Evaluation Studies," Proc. 4th Conf. on Gas Turbine Materials in the Marine Environment (1979).

LBL Reports

1. I. M. Allam, H. C. Akuezue, and D. P. Whittle, "Influence of Small Pt Additions on Al_2O_3 Scale Adherence," LBL-9180.

2. I. M. Allam, D. P. Whittle and J. Stringer, "The Role of Active Elements and Oxide Dispersions in the Development of Oxidation-Resistant Alloys and Coatings," LBL-9516.

3. G. W. Roper and D. P. Whittle, "Multicomponent Diffusion," LBL-9758.

4. O. T. Goncel, D. P. Whittle, and J. Stringer, "The Oxidation Behavior of Fe-Cr Alloys Containing HfO_2 - Dispersed Phase," LBL-9709.

5. D. P. Whittle and A. V. Levy, "Oil Shale Retort Components," LBL-9792.

6. T. Hadishi, A. V. Levy, D. P. Whittle and E. Cuellar, "Determination of S_2 in Reactive Gas Mixtures by Tunable Atomic Line Molecular Spectroscopy," LBL-9678.

7. R. Stanley, D. P. Whittle, and A. V. Levy, "Characterization of the Degradation of Hydrodesulfurizing Catalysts," LBL-10026.

8. D. P. Whittle, F. Gesmundo, D. D. Bastow, and G. C. Wood, "Formation of Subscales of Varying Composition," LBL-10067.

9. H. C. Akuezue, "Calcium Sulfate-Induced Accelerated Corrosion," (M.S. thesis), LBL-10286.

Invited Talks

1. I. M. Allam, D. P. Whittle, and J. Stringer, "Improved Adhesion of Al_2O_3 Scales on CoCrAl Alloys," poster paper, Gordon Research Conf. on Corrosion, New London, New Hampshire, July 1979.

2. F. Gesmundo, F. Vianni, and D. P. Whittle, "High Temperature Oxidation of Two Phase Alloys," poster paper, Gordon Research Conf. on Corrosion, New London, New Hampshire, July 1979.

3. A. K. Misra and D. P. Whittle, "Hot Corrosion of Nickel-Base Alloys at Intermediate Temperatures," Electrochem. Soc. Meeting, Los Angeles, California, October 1979.

4. D. P. Whittle, "The Importance of the Metal/Scale Interface in High Temperature Oxidation," DOE Meeting on Microchemical and Microstructural Analysis of Minority and Interface Phases, Germantown, Maryland, May 1979.

5. K. N. Strafford, D. P. Whittle, P. J. Hunt, and A. K. Misra, "The Corrosion of M-Cr-Al-Y type Alloys: Evaluation Studies," 4th Conf. on Gas Turbine Materials in a Marine Environment, Annapolis, Maryland, June 1979.

6. T. Hadeishi, A. V. Levy, D. P. Whittle, and E. Cuellar, "Determination of S_2 in Reactive Gas Mixtures by Tunable Atomic Line Molecular Spectroscopy," 1979 Symposium on Instrumentation and Control for Fossil Energy Processes, Denver, Colorado, August 1979.

This report was done with support from the United States Energy Research and Development Administration. Any conclusions or opinions expressed in this report represent solely those of the author(s) and not necessarily those of The Regents of the University of California, the Lawrence Berkeley Laboratory or the United States Energy Research and Development Administration.